Title
Mitochondrial alarmins released by degenerating motor axon terminals activate perisynaptic Schwann cells

Journal
Proceedings of the National Academy of Sciences of the United States of America, 112(5)

ISSN
0027-8424

Authors
Duregotti, Elisa
Negro, Samuele
Scorzeto, Michele
et al.

Publication Date
2015-02-03

DOI
10.1073/pnas.1417108112

Peer reviewed

PNAS PLUS

Mitochondrial alarmins released by degenerating motor axon terminals activate perisynaptic Schwann cells

Elisa Duregotti[a], Samuele Negro[a], Michele Scorzeto[a], Irene Zornetta[a], Bryan C. Dickinson[b,c,1], Christopher J. Chang[b,c], Cesare Montecucco[a,d,2], and Michela Rigoni[a,2]

[a]Department of Biomedical Sciences, University of Padua, Padua 35131, Italy; [b]Department of Chemistry and Molecular and Cell Biology and [c]Howard Hughes Medical Institute, University of California, Berkeley, CA 94720; and [d]Italian National Research Council Institute of Neuroscience, Padua 35131, Italy

Edited by Thomas C. Südhof, Stanford University School of Medicine, Stanford, CA, and approved December 22, 2014 (received for review September 5, 2014)

An acute and highly reproducible motor axon terminal degeneration followed by complete regeneration is induced by some animal presynaptic neurotoxins, representing an appropriate and controlled system to dissect the molecular mechanisms underlying degeneration and regeneration of peripheral nerve terminals. We have previously shown that nerve terminals exposed to spider or snake presynaptic neurotoxins degenerate as a result of calcium overload and mitochondrial failure. Here we show that toxin-treated primary neurons release signaling molecules derived from mitochondria: hydrogen peroxide, mitochondrial DNA, and cytochrome c. These molecules activate isolated primary Schwann cells, Schwann cells cocultured with neurons and at neuromuscular junction in vivo through the MAPK pathway. We propose that this inter- and intracellular signaling is involved in triggering the regeneration of peripheral nerve terminals affected by other forms of neurodegenerative diseases.

motor axon degeneration | presynaptic neurotoxins | mitochondrial alarmins | Schwann cells

The venoms of the black widow spider *Latrodectus mactans*, the Australian taipan snake *Oxyuranus scutellatus scutellatus*, and the Taiwan krait *Bungarus multinctus* cause the paralysis of peripheral skeletal and autonomic nerve terminals in envenomated subjects. Such paralysis is completely reversible, and within a month or so, patients, supported by mechanical ventilation, recover completely (1–3). Paralysis in mice/rodents has a shorter duration, and again recovery is complete (4, 5). Major presynaptic toxins of these venoms are α-latrotoxin (α-Ltx), taipoxin (Tpx), and β-bungarotoxin (β-Btx), respectively (6, 7). α-Ltx induces a very rapid nerve terminal paralysis by forming transmembrane ion channels that cause a massive Ca^{2+} entry, with exocytosis of synaptic vesicles and mitochondrial damage (7–11). This is followed by Ca^{2+}-induced degeneration of motor axon terminals, which is remarkably limited to the unmyelinated endplate. Complete regeneration is achieved in mice within 8–10 d (4). Tpx and β-Btx are representative of a large family of presynaptic snake neurotoxins endowed with phospholipase A2 activity (SPANs), which are important, although neglected, human pathogens (12–15). We have contributed to the definition of their mechanism of action, which involves generation of lysophospholipids and fatty acids on the external layer of the plasma membrane (16, 17). The mixture of these lipid products favors exocytosis of ready-to-release synaptic vesicles and mediates the rise of cytosolic Ca^{2+}, presumably via transient lipid ion channels (16, 18). In turn, this Ca^{2+} influx causes a massive release of synaptic vesicles and mitochondrial damage, with ensuing complete degeneration of axon terminals (5, 18–20). Similar to α-Ltx, SPANs-induced peripheral paralysis is followed by a complete recovery: regeneration and functional reinnervation are almost fully restored in rats by 5 d (20). The similar outcome and time-course of the paralysis induced by the two types of presynaptic neurotoxins suggest that the common property of inducing Ca^{2+} entry into the nerve terminals is the main cause of nerve terminal degeneration (21). Indeed, these neurotoxins cause activation of the calcium-activated calpains that contribute to cytoskeleton fragmentation (22).

Although clearly documented (4, 5, 20), the regeneration of the motor axon terminals after presynaptic neurotoxins injection is poorly known in its cellular and molecular aspects. Available evidence indicates that, in general, regeneration of mechanically damaged motor neuron terminals relies on all three cellular components of the neuromuscular junction (NMJ): the neuron, the perisynaptic Schwann cells (PSCs), and the muscle cells (23, 24). The regeneration steps that take place on animal neurotoxin poisoning are likely to be similar to those after the cut or crush of nerves, as a closely similar cascade of toxic events occurs in both conditions (i.e., calcium overload, mitochondrial impairment, and cytoskeleton degradation). Similar neurodegenerative events are also shared by traumatized patients. However, the model system used here provides the advantage of being much more controlled and more reproducible. In addition, it does not involve the death of many cell types, as it follows a well-characterized biochemical lesion of the end plate only (7, 8, 10–12, 16, 18). Therefore, the mouse NMJ treated with α-Ltx, Tpx, or β-Btx represents a relevant model of acute motor axon terminal

Significance

The neuromuscular junction is the site of transmission of the nerve impulse to the muscle. This finely tuned synapse relies on at least three components: the motor neuron, the muscle fiber, and the Schwann cells, which assist nerve recovery after injury. Using animal neurotoxins to induce an acute and reversible nerve degeneration, we have identified several mitochondrial molecules through which the damaged nerve terminal communicates with nearby cells, activating signaling pathways in Schwann cells involved in nerve regeneration. Among these messengers, hydrogen peroxide appears to be crucial at the initial stages of regeneration, because its inactivation delays the functional recovery of the damaged neuromuscular junction in vivo. These findings provide important indications about the pharmacological treatment of traumatized patients.

Author contributions: C.M. and M.R. designed research; E.D., S.N., M.S., and I.Z. performed research; B.C.D. and C.J.C. contributed new reagents/analytic tools; E.D., S.N., M.S., I.Z., C.M., and M.R. analyzed data; and E.D., S.N., M.S., I.Z., B.C.D., C.J.C., C.M., and M.R. wrote the paper.

The authors declare no conflict of interest.

This article is a PNAS Direct Submission.

Freely available online through the PNAS open access option.

[1]Present address: Gordon Center for Integrative Sciences, University of Chicago, Chicago, IL 60637.

[2]To whom correspondence may be addressed. Email: michela.rigoni@unipd.it or cesare.montecucco@unipd.it.

This article contains supporting information online at www.pnas.org/lookup/suppl/doi:10.1073/pnas.1417108112/-/DCSupplemental.

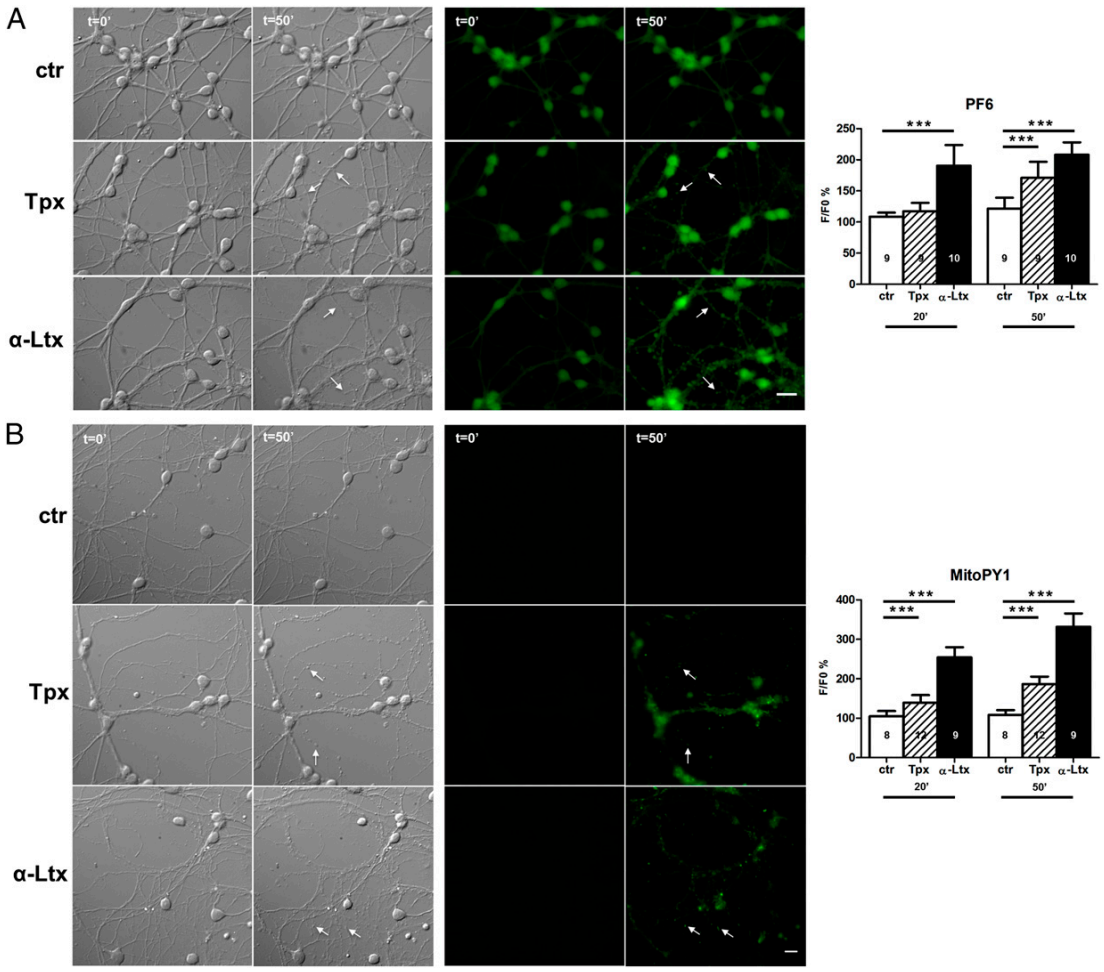

Fig. 1. Live-imaging of neuronal hydrogen peroxide production. Rat CGNs were loaded with the H_2O_2-specific probes PF6-AM (*A*) or MitoPY1 (*B*), washed, and then exposed to Tpx 6 nM or α-Ltx 0.1 nM for 50 min. Changes in fluorescence resulting from H_2O_2 production were monitored with time and expressed as a percentage of the fluorescence value at $t = 0$ (*Right*). ***$P < 0.001$. Arrows in bright-field images and in the green channel point to neuronal bulges. (Scale bars: 10 μm.)

degeneration and regeneration, which is likely to provide information useful to the understanding of the pathogenesis not only of envenomation but also, more in general, of other human pathological syndromes.

Cell death and injury often lead to the release or exposure of intracellular molecules called damage-associated molecular patterns (DAMPs) or alarmins. Recently, mitochondria have emerged as major sources of DAMPs (25). Mitochondria are abundant subcellular components of the NMJ that have been recently shown to release mitochondrial DNA (mtDNA) and cytochrome c (Cyt c) after trauma or snake myotoxin-induced muscle damage, thus contributing to the systemic or local inflammatory responses associated with such conditions (26, 27). In this study, we tested whether α-Ltx and SPANs induce the release of mitochondrial signaling molecules from primary neuronal cultures and found that, in addition to mtDNA and Cyt c, hydrogen peroxide (H_2O_2) is released. First candidate targets of these mitochondrial mediators released by damaged neurons are nonmyelinating PSCs, which are intimately associated with the end plate. They play an active role in the formation, function, maintenance, and repair of the NMJ (28–33). PSC activation parallels nerve degeneration and contributes to neuronal regeneration by phagocytosis of cellular debris and by extension of processes that guide reinnervation (34, 35). We therefore investigated whether mitochondrial DAMPs released by injured neurons were able to activate SCs, and through which downstream pathway. Using isolated primary cells, neuron-Schwann cell cocultures, and the NMJ in vivo, we found that PSCs are activated by mitochondrial alarmins and that the MAPK signaling pathway is involved in this process.

Results

Hydrogen Peroxide Is Produced by Neurons Exposed to Spider or Snake Presynaptic Neurotoxins. Given that mitochondria of stressed cells produce superoxide anion, which is rapidly converted into H_2O_2, and that in neurons exposed to the neurotoxins, mitochondria functionality is impaired, we asked whether intoxication of neurons by α-Ltx or SPANs leads to H_2O_2 production, an ideal candidate as intercellular signaling molecule (36–38). We therefore loaded rat cerebellar granular neurons (CGNs) with specific H_2O_2 probes with different cellular localization and monitored the samples for up to an hour. MitoPY1 is a bifunctional molecule that combines a chemoselective boronate-based switch and a mitochondrial-targeting phosphonium moiety for the detection

of H_2O_2 localized to mitochondria (39). PF6-AM takes advantage of multiple masked carboxylates to increase cellular retention, and hence sensitivity to low levels of peroxide. In its ester-protected form, PF6-AM can readily enter cells. Once inside cells, the protecting groups are rapidly cleaved by intracellular esterases to produce their anionic carboxylate forms, which are effectively trapped within cells (40).

After exposure to α-Ltx or Tpx, H_2O_2 levels increased with time, markedly at the level of neurite enlargements (so-called bulges), which are a hallmark of intoxication (16, 41), as shown in Fig. 1. Bulges are sites of calcium overload and accumulation of depolarized mitochondria (18), and the MitoPY1 signal indicates that these mitochondria produce H_2O_2. Quantification of the signals indicates a more pronounced effect of α-Ltx with respect to Tpx, in agreement with the fact that the pore formed by the former neurotoxin mediates a larger Ca^{2+} entry than Tpx (21). Similar results were obtained following intoxication of rat spinal cord motor neurons (MNs; Fig. S1). That mitochondria are the major source of H_2O_2 is reinforced by the finding that toxins failed to induce membrane translocation of cytoplasmic p47phox, a regulatory component of the NADPH oxidase complex, which excludes a role of the NADPH oxidase system (Fig. S2).

Hydrogen Peroxide Released by Degenerating Nerve Terminals Activates Schwann Cells and Stimulates Regeneration. Growing evidence indicates that H_2O_2 is a largely used intercellular signaling molecule regulating kinase-driven pathways (37, 38, 42): it triggers ERK phosphorylation in different cell types (43), with consequent activation of downstream gene transcription, and ERK signaling was recently shown to play a central role in the orchestration of axon repair by SCs (44, 45).

In preliminary experiments, we checked whether primary SCs isolated from rat sciatic nerves were responsive to H_2O_2 by analyzing ERK phosphorylation by Western blotting and immunofluorescence. Exposure of primary SCs to H_2O_2 led to ERK phosphorylation and translocation of p-ERK into the nucleus (Fig. S3 *A* and *B*). Cocultures of primary spinal cord motor neurons and sciatic nerve-derived SCs were then exposed to α-Ltx or Tpx: bulges appeared within few minutes along neuronal processes, and p-ERK was detected in the cytoplasm and nucleus of SCs (Fig. 2*A*). Phospho-ERK-positive cells were also positive for S-100, a specific SC marker (Fig. S3*C*). In cocultures, the score of S-100-positive cells that become p-ERK-positive is 59% on intoxication with β-Btx ($n = 81$) and 78% in the case of α-Ltx ($n = 69$). These percentages were obtained by counting many S-100-positive cells randomly distributed in different fields, but the value is actually much higher if one considers only clustered SCs in close proximity of intoxicated neurites; this observation further supports the conclusion that molecules released by injured neurons reach nearby SCs, thus activating them.

ERK phosphorylation was reduced in cocultures preincubated with catalase, which converts H_2O_2 into water and O_2, indicating that H_2O_2 produced inside neurons diffuses to reach nearby SCs, contributing to their ERK activation (Fig. 2*B*). Residual p-ERK signal might be a result of mediators other than H_2O_2 released on neuronal injury. Toxins failed to induce a direct ERK phosphorylation either in isolated SCs (Fig. S3*D*) or in isolated primary neurons (Fig. 2*B*).

Next we tested whether the ERK pathway is activated also within PSCs at the NMJs of intoxicated mice. Sublethal doses of the neurotoxins were s.c. injected in transgenic mice expressing a cytoplasmic GFP specifically in SCs under the *plp* promoter (46, 47), in proximity to the levator auris longus (LAL) (48), a thin muscle ideal for imaging. Twenty-four hours later, muscles were collected and processed for indirect immunohistochemistry. A clear p-ERK signal was detected at the level of PSCs in treated NMJs, thus extending in vivo the results obtained in cocultures

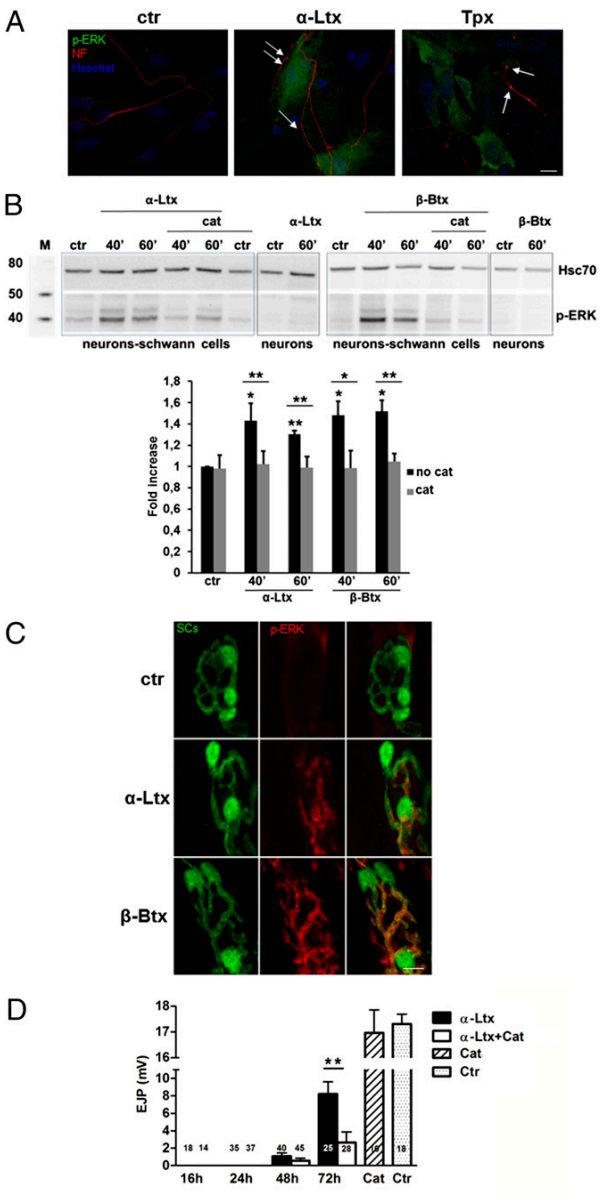

Fig. 2. Hydrogen peroxide released after nerve terminal degeneration activates ERK in Schwann cells and stimulates regeneration. Phospho-ERK (green) was detected in primary SCs cocultured with spinal cord MNs on exposure to α-Ltx (0.1 nM) or SPANs (6 nM) for 50 min by immunofluorescence (*A*), as well as by Western blots of total lysates (*B*). Arrows in *A* point to neuronal bulges stained with an antibody against neurofilaments (NF; red). Nuclei are stained with Hoechst (blue). (Scale bars: 10 μm.) (*B*) Catalase pretreatment of cocultures (1,000 U) significantly reduced ERK phosphorylation induced by the toxins (Western blot and quantification). No ERK phosphorylation is induced in neurons by the toxins. $*P < 0.05$; $**P < 0.01$; $n = 4$. (*C*) α-Ltx or β-Btx s.c. injections in LAL muscle of transgenic mice trigger ERK phosphorylation (p-ERK; red) in PSCs (green). Muscles were collected 24 h after injection. (Scale bars: 10 μm.) *(D)* Electrophysiological recordings of EJPs at soleus NMJs treated with α-Ltx alone (5 μg/kg; black bars) or with α-Ltx plus catalase (750 U; white bars). At 72 h EJP amplitudes of fibers exposed to toxin plus catalase are significantly smaller than those exposed to the sole toxin ($**P < 0.01$).

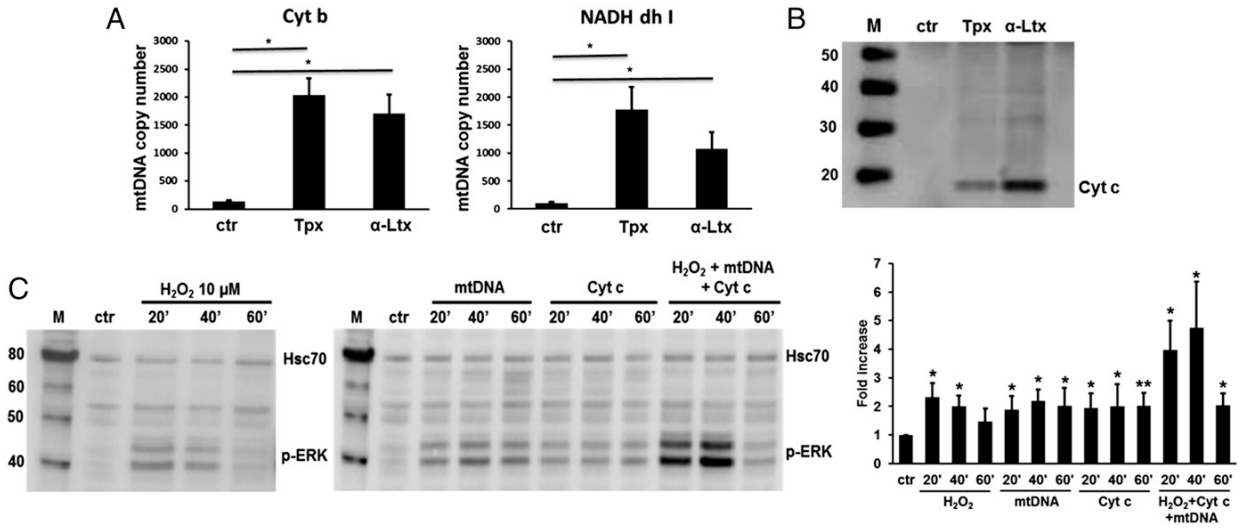

Fig. 3. Mitochondrial DNA and cytochrome *c* are released by degenerating neurons and activate the ERK pathway, together with hydrogen peroxide. (*A*) Real-time qPCR performed on CGNs supernatants from control and toxin-treated samples (Tpx 6 nM or α-Ltx 0.1 nM for 50 min), using primers specific for rat mitochondrial genes Cyt b and NADH dhI. DNA copy numbers of control and treated samples have been quantified. $*P < 0{,}05$; $n = 11$. (*B*) Supernatants from control and neurons treated as described earlier were precipitated with TCA and probed for Cyt c immunoreactivity in Western blot. (*C*) Time-course of ERK-phosphorylation induced in primary SCs by H_2O_2 (10 μM), mtDNA (10 μg/mL), and Cyt c (1 μg/mL) added alone or in a mixture and the relative quantification. Phospho-ERK signal was normalized to the Hsc70 band. $*P < 0.05$; $**P < 0.01$; $n = 3$.

(Fig. 2*C*). The importance of ERK pathway for SCs activation and regeneration was addressed by a pharmacologic approach: SCs-MNs cocultures exposed to the neurotoxins show a decreased ERK phosphorylation in the presence of the MEK 1 inhibitor PD98059 (Fig. S4 *A* and *B*); moreover, soleus muscles of mice pretreated with PD98059 and then locally injected with α-Ltx show a delayed recovery from paralysis with respect to mice injected with toxin only (Fig. S4*C*).

PSCs respond to neurotoxin-induced nerve degeneration by forming long sproutings and bridges between junctions of different fibers by the first day of injection (Fig. S5). This response has been long known to follow nerve terminal damage (35), and therefore, the present toxin-based model of acute nerve degeneration reproduces the known crucial aspects of regeneration.

To test whether H_2O_2 production by injured nerve terminals is important for functional regeneration, we performed electrophysiological recordings at soleus NMJs 16, 24, 48, and 72 h after i.m. injections of α-Ltx alone or α-Ltx plus catalase. Three days after treatment, fibers injected with α-Ltx plus catalase showed evoked junction potentials (EJPs) with significantly smaller amplitudes than those injected only with the toxin, indicating a slowdown of the regeneration process; muscles treated with catalase alone showed EJPs indistinguishable from the control (Fig. 2*D*). Immunohistochemistry on LAL muscles treated as described earlier confirmed the electrophysiological results, showing a delay in the recovery of synaptosomal-associated protein 25 (SNAP-25) staining, a presynaptic marker, in samples exposed to α-Ltx plus catalase compared with muscles injected with α-Ltx only (Fig. S6). At 24 h, SNAP-25 staining is recovered in 80% of the NMJs treated with α-Ltx (90% at 48 h) compared with 17% of the NMJs treated with α-Ltx plus catalase (33% at 48 h; $n = 40$). The disappearance of SNAP-25 during the degeneration steps takes place with a closely similar kinetic under the two conditions (Fig. S6). Four hours after intoxication, SNAP-25 displays a spotty distribution in nearly all NMJs analyzed (indicative of nerve terminal degeneration), both in the presence and absence of catalase; at 16 h, 68% of α-Ltx-treated NMJs have no more SNAP-25 versus 60% of catalase and α-Ltx-treated NMJs ($n = 30$).

mtDNA and Cyt C Are Released by Degenerating Neurons and Activate the ERK Pathway in Schwann Cells. We next tested whether mtDNA and Cyt c could act together with H_2O_2 as neuronal mediators of PSCs activation. For mtDNA detection, primary neurons were intoxicated, the supernatants collected, and DNA purified. The eluates were subjected to real-time PCR, using primers specific for the rat mitochondrial genes Cyt b and NADH dhI. Fig. 3*A* shows that mtDNA is indeed released in the neuronal supernatant after treatment with Tpx or α-Ltx. In another set of experiments, TCA-precipitated cell supernatants (sham or toxin-treated) were loaded in SDS/PAGE, followed by Western blotting. Samples were probed with an antibody against Cyt c: only toxin-treated samples showed a clear band corresponding to the intact, monomeric form of the protein (Fig. 3*B*). Control experiments showed no amplification when primers for the nuclear gene GAPDH were used (Fig. S7*A*), and the LDH assay on neuronal supernatant excluded a loss of membrane integrity (Fig. S7*B*). Thioredoxin 2, a mitochondrial protein with a molecular weight similar to Cyt c, was undetectable by Western blot of toxin-treated supernatants precipitated with TCA, thus supporting the conclusion that neuronal alarmins are released from intact membranes (Fig. S7*C*). Moreover, CGNs loaded with calcein-AM did not lose dye during 50 min incubation with both the toxins, indicating conservation of plasma membrane integrity (Fig. S7*D*).

Exposure of isolated SCs to mtDNA or Cyt c led to a sustained ERK phosphorylation, whereas a peak of p-ERK followed by progressive decline was observed upon H_2O_2 stimulation. When the three mitochondrial alarmins were added together, an additive effect on ERK phosphorylation was observed (Fig. 3*C*).

Mitochondrial Alarmins Exit from Neurons. H_2O_2 is permeable to biological membranes (49), whereas mtDNA and Cyt c must be released from mitochondrial and plasma membranes to reach the extracellular medium. Pretreatment of neurons with cyclosporin A, a drug that desensitizes the mitochondrial permeability transition pore (PTP) via its binding to cyclophilin D (50), reduces both mtDNA and Cyt c release triggered by the toxins (Fig. 4 *A* and *B*), suggesting these molecules can exit mitochondria and

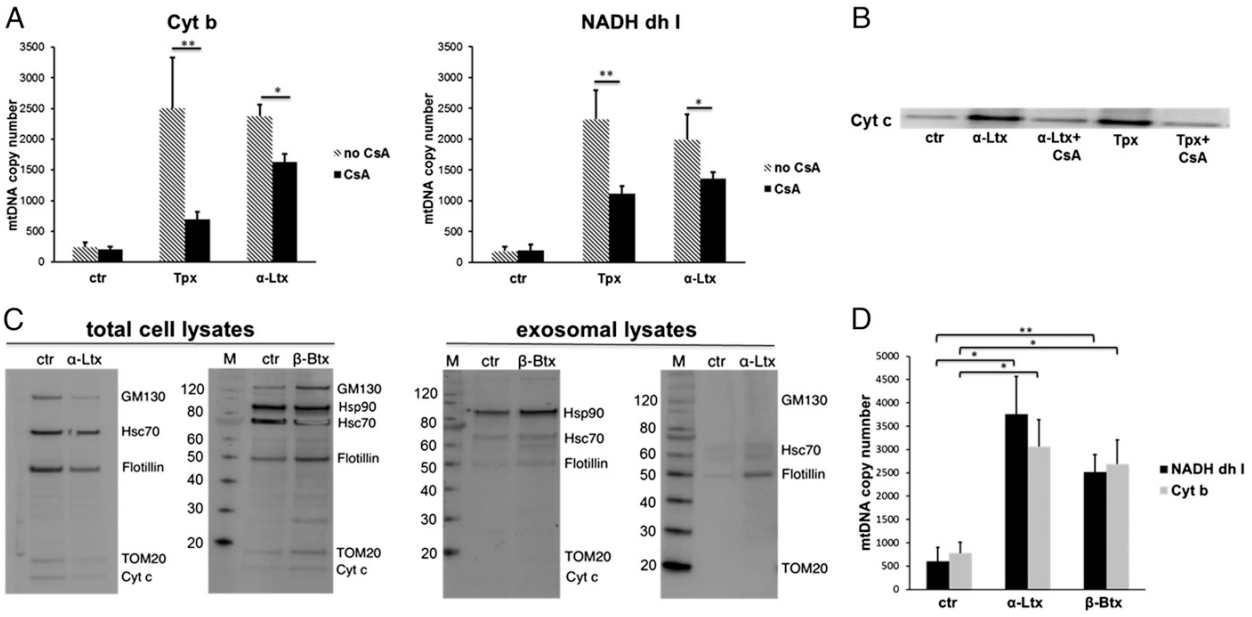

Fig. 4. Mitochondrial alarmins exit from neurons. Preincubation with cyclosporine A (5 μM for 30 min) significantly reduced both mtDNA (*A*) and Cyt c release (*B*) induced by exposure of CGNs to Tpx or α-Ltx (6 nM and 0.1 nM for 50 min, respectively). $*P < 0.05$; $**P < 0.01$; $n = 3$. (*C*) Exosomes were purified from CGNs supernatants and probed for the exosome-enriched proteins flotillin, Hsc70, and Hsp90. The absence of the Golgi marker GM130 and of the mitochondrial one Tom20 is indicative of uncontaminated preparations (*Right*). Cellular lysates are positive for all markers tested (*Left*). (*D*) DNA was extracted from exosomes purified from the supernatants of α-Ltx- and β-Btx-treated CGNs (0.1 and 6 nM for 50 min, respectively) and subjected to real-time qPCR for the detection of mtDNA. $*P < 0.05$; $**P < 0.01$; $n = 5$.

reach the cytoplasm through the PTP, whose opening is indeed induced by snake neurotoxins (51).

Because neuronal plasma membrane integrity is preserved, how do these alarmins reach the extracellular medium? We posited that exosomes might be involved and have purified them from control and treated neuronal supernatants. Purified exosomes were found enriched in Hsp90, Hsc70, flotillin, and CD63; no contamination with Golgi, mitochondrial, or plasma membranes was detected (Fig. 4*C* and Fig. S8 *A* and *B*). Electron microscopy and immunogold labeling of purified exosomes confirmed their correct morphology, size, and positivity for Hsp90 (Fig. S8*C*). Next, we purified total DNA from exosomes and performed real-time PCR to check for their mtDNA content. Fig. 4*D* shows that exosomes released by α-Ltx- and β-Btx-intoxicated neurons do contain mtDNA. Similar mtDNA copy numbers were found before and after DNase treatment of exosomal fractions, indicating that mtDNA is indeed inside exosomes (Fig. S8*D*). In contrast, no Cyt c was detected in exosomes by Western blotting; this is likely to be a result of the much lower sensitivity of Western blotting with respect to RT-PCR, but the possibility that Cyt c is released from damaged nerve terminals via other mechanisms cannot be discarded.

Phagocytosis Is Induced in PSCs During Nerve Terminal Injury. During toxin-induced neurodegeneration, PSCs at poisoned NMJs undergo evident morphological changes, showing a number of intracellular structures appearing dense by light microscopy (Fig. 5*A*, *Lower*). These structures are particularly evident at 4 h after α-Ltx injection, with a reduction in number and size with time (Fig. 5*A*).

The appearance and life span of these structures parallel nerve terminal degeneration, suggesting they might be phagosomes involved in the clearance of nerve debris. Accordingly, immunostaining of sham or poisoned LAL muscles for the scavenger macrophage receptor CD68 was performed. After α-Ltx injection, perineural SCs of LAL NMJs do express CD68 on these intracellular structures, supporting their phagocytic role (Fig. 5*B*). CD68-positive structures also appear after β-Btx treatment, but at a later time (16 h), as expected on the basis of the different time course of pathogenesis of the two neurotoxins (Fig. 5*B*). Lysotracker-positive staining confirmed the acidic nature of such compartments (Fig. 5*C*). CD68-positive macrophages were also recruited in the proximity of neurotoxin-treated NMJs, with a typical migrating phenotype (Fig. S9); this is consistent with the chemoattractant role of H_2O_2 (52–54). In contrast, polymorphonuclear leukocytes, which are recruited by axonal degradation (54), were rarely seen in the many samples we have inspected.

Four hours after α-Ltx injection, the distribution of the presynaptic markers neurofilaments (NF) and SNAP-25 is altered, with clear fragmentation in many junctions, as a result of the specific and localized nerve terminal degeneration induced by the neurotoxins (Fig. 6 *A* and *B*). SNAP-25-positive spots localize within PSCs phagosomes (the same holds true for NF), as shown by orthogonal projections (Fig. 6*C*), confirming that phagocytosis by PSCs and macrophages is taking place during nerve terminal degeneration.

Discussion

The present article describes an original approach to study motor axon terminals degeneration and regeneration. This model system is based on the use of animal presynaptic neurotoxins highly specific for nerve terminals with a well-defined biochemical mechanism of action (10, 12, 16, 18). Here, these neurotoxins are used as tools to induce localized and reversible nerve degeneration, followed by complete regeneration. This system is more controllable than the classical cut and crush approaches, which are invasive and inevitably damage several cell types, triggering a pronounced inflammatory response (55). Moreover, this model avoids some adverse effects of techniques such as laser ablation (high temperatures, photooxidation, etc). The model proposed here is therefore better suited to

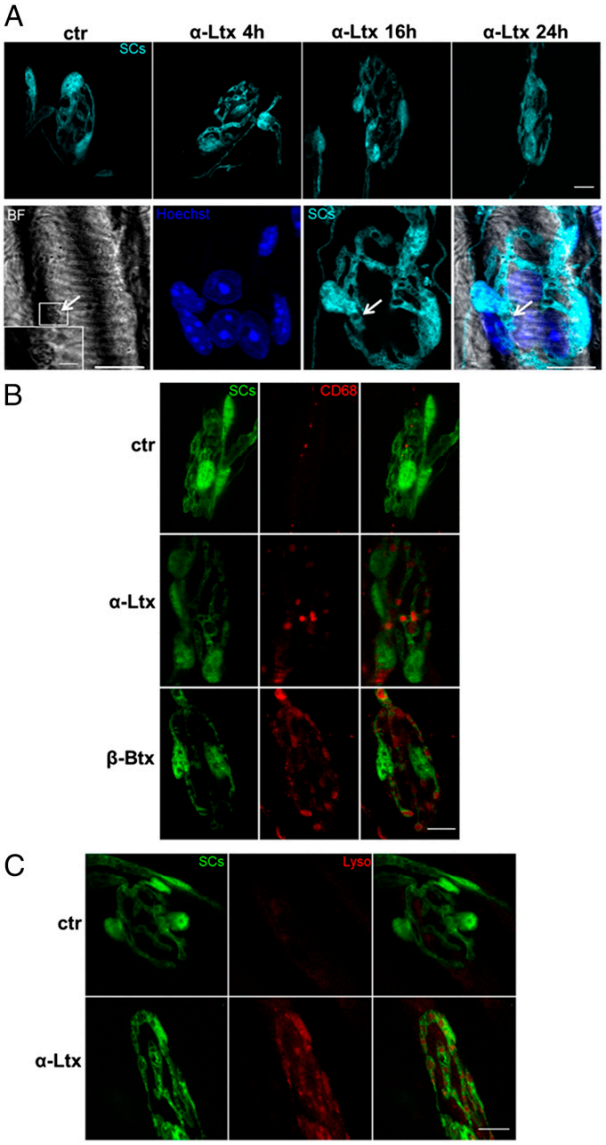

Fig. 5. Nerve terminal degeneration triggers phagocytosis in terminal SCs at the NMJ. (*A*) LAL muscles from transgenic mice were injected with α-Ltx (5 μg/kg), collected at different time points (4, 16, 24 h), and processed for indirect immunohistochemistry. PSCs (cyan) show intracellular structures of different size that are particularly evident after 4 h of intoxication. These structures appear dense by light microscopy (brightfield, *Lower*, arrows). Nuclei are stained with Hoechst (blue). (Scale bars: 10 μm.) (*B*) PSCs (green) at α-Ltx- and β-Btx-treated NMJs (4 and 16 h of intoxication, respectively) are positive for the phagocytic marker CD68 (red), which stains intracellular vesicular structures. A very low CD68 signal is detected in control NMJs. (Scale bars: 10 μm.) (*C*) Ex vivo Lysotracker staining (red) of α-Ltx-treated LAL (4 h) confirms the acidic nature of intracellular vacuoles. (Scale bar: 10 μm.)

study the inter- and intracellular signaling and transcriptomic events involved in the regeneration process.

Spider and snake presynaptic neurotoxins induce, by different biochemical mechanisms, a large entry of calcium in axon terminals, which in turn leads to mitochondrial failure and nerve terminal degeneration. At the same time, PSCs perceive the damage occurring to the motor axons and respond by dedifferentiating to a progenitor-like state, proliferating and assisting nerve regeneration. They acquire macrophagic-like activities that contribute to the removal of nerve cell debris and facilitate reinnervation, similar to what was found previously after nerve crush (23). Moreover, upon extensive cytoskeletal reorganization, PSCs send out long projections, along which the regenerating nerve terminals extend sprouts, which originate from the nonmyelinated axon terminal to innervate adjacent denervated junctions (34, 35).

It was recently shown that the MAPK signaling pathway has a central role in controlling SC plasticity and peripheral nerve regeneration via the activation of ERK1/2 and JNK, which activate the transcription complex activator protein 1, of which c-Jun is a key component (44, 45, 56). The major result obtained here, using p-ERK as a read-out, is that alarmins released by mitochondria of degenerating axon terminals activate SCs. Mitochondria are abundant components of the motor axons terminals, and here we define them as a source of mediators that are released under cytosolic calcium overload. The rapid accumulation of Ca^{2+} inside mitochondria causes the opening of the PTP and the exit of alarmins (50). Mitochondrial alterations are hallmarks of nerve terminal damage (19, 20), and therefore the present findings can be extrapolated to several other nerve terminal pathological conditions.

Mitochondria of stressed cells produce reactive oxygen species (ROS), among which H_2O_2 is the most stable species (37, 38, 57). It is a very reactive molecule that can permeate biological membranes. As PSCs and axon terminals are in close contact within the NMJ, significant amounts of H_2O_2 released by axon terminals can reach PSCs before it becomes inactivated by cellular antioxidant defense systems. Once within the target cell, H_2O_2 can act as a second messenger via chemoselective oxidation of cysteine residues in signaling proteins and via ERK phosphorylation. Collectively, these properties make H_2O_2 an ideal mediator of signal transduction processes (36–38, 42, 58). Recent experimental

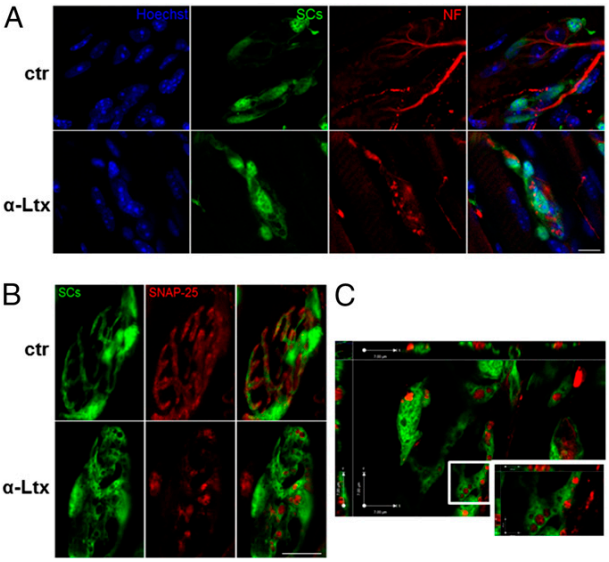

Fig. 6. Degenerating terminals are engulfed by perisynaptic SCs. (*A*) PSCs engulf presynaptic components, as shown by NF-positive staining of PSCs phagosomes at NMJs treated for 4 h with α-Ltx (red, *Lower*). (*Upper*) control NMJs. Nuclei are stained with Hoechst (blue). (Scale bars: 10 μm.) (*B*) Control NMJs with typical SNAP-25 presynaptic localization (red). In α-Ltx-treated NMJs (4 h), SNAP-25 aggregates localize within PSC phagosomes. (Scale bars: 10 μm.) (*C*) Orthogonal projections of α-Ltx-treated NMJs show that SNAP-25 positive aggregates are inside PSCs phagosomes. (Scale bars: 10 μm.)

evidence in different animal models demonstrated that a rapid concentration gradient of H_2O_2 is generated during injury and that H_2O_2 is a powerful chemoattractant of leukocytes (53, 54). Moreover, lowering ROS levels by pharmacologic or genetic approaches reduces cell proliferation and impairs regeneration (59). We therefore have imaged H_2O_2 in living neurons exposed to neurotoxins with novel specific fluorescent probes (39, 40) and found that the degenerating nerve terminals release H_2O_2 of mitochondrial origin. This H_2O_2 activates PSCs in vitro and in vivo. We also found that macrophages are recruited around the neurotoxin-treated NMJs. It is therefore likely that these macrophages are attracted by H_2O_2, as well as by molecules released by activated PSCs, as previously found (60, 61). The prominent role of H_2O_2 in neurotoxin-induced nerve degeneration and repair is proved by the impaired regeneration we observed in the presence of catalase.

In addition to H_2O_2, we found that mtDNA and Cyt c can act as mediators of neuronal damage and activate SCs via ERK pathway. When added in a mixture with H_2O_2, an additive effect on ERK phosphorylation is observed. As neuronal membrane integrity is preserved, the question arises of how mtDNA and Cyt c, coming from the mitochondrial matrix or the intermembrane space, respectively, can exit the cell. Several pieces of evidence indicate that mitochondria are central sensors for axonal degenerative stimuli (62), and the release of mtDNA fragments from PTP in isolated mitochondria has been documented (63). Here, the mitochondrial PTP was found to be involved in the exit of both mtDNA and Cyt c from mitochondria, with a significant reduction in the presence of the PTP desensitizing molecule cyclosporin A. Once in the cytosol, mtDNA and Cyt c could be released via the nonclassical or unconventional secretory route, including secretory lysosomes, membrane blebbing, multivesicular body-derived exosomes, or autophagy (64). Here, we found that exosomes purified from intoxicated neuronal supernatants contain mtDNA, whereas Cyt c was not detected, possibly because of the insufficient sensitivity of Western blot. It is also possible that Cyt c is released directly via contact sites between mitochondria and the presynaptic membrane, similar to those observed by electron microscopy in a closely similar pathological condition caused by autoimmune anti-ganglioside antibodies (65).

The present work has identified three mitochondrial alarmins involved in PSCs activation after an acute nerve injury and proposes H_2O_2 as the strongest inducer of PSCs response. Inactivation of H_2O_2 by catalase reduces ERK phosphorylation in SCs in culture and delays NMJ recovery in vivo after toxin-induced neuroparalysis and degeneration, supporting a crucial role of this molecule in the regeneration process.

Nerve damage triggers important morphologic and functional changes in PSCs aimed at promoting NMJ regeneration, confirming their endowed high plasticity and their crucial role in the clearance of nerve debris. Indeed, during nerve terminal degeneration, PSCs become CD68-positive, indicating an acquired phagocytic activity. Together with macrophages, but not neutrophils, activated PSCs were found here to remove nerve debris, thus permitting a functional nerve regeneration. This is at variance from what was found during axonal degeneration, where a pronounced neutrophil infiltration was detected (54).

The phagocytic features of PSCs described here represent an additional early read-out of PSCs activation at the injured NMJ. PSCs respond to axonal damage caused by neurotoxin poisoning by engulfing degenerating terminals, by extending long processes, and by activating intracellular signaling pathways crucial for regeneration. On the basis of these perspectives, we plan to study more in detail the intracellular signaling and transcriptomic events taking place inside activated PSCs. More in general, it appears that the present experimental approach can be extended to the investigation of other motor neuron diseases, including the non-cell-autonomous and dying-back axonopathy of ALS and autoimmune neuropathies including Guillain-Barré and Miller-Fisher syndromes (66, 67). Such studies are likely to provide relevant insights for future therapeutic endeavors.

Materials and Methods

Animal Strains. C57BL/6 mice expressing cytosolic GFP under the *plp* promoter (46, 47) were kindly provided by W. B. Macklin (Aurora, CO) via the collaboration of T. Misgeld (Munchen, Germany). All experiments were performed in accordance with the European Communities Council Directive n° 2010/63/UE and approved by the Italian Ministry of Health.

Hydrogen Peroxide Detection. Hydrogen peroxide generation in primary neurons was measured using Mitochondria Peroxy Yellow 1 (MitoPY1) (39) or Peroxyfluor 6 acetoxymethyl ester (PF6-AM) (40), synthesized in the C.J.C. laboratory (Berkeley, CA), specific probes of H_2O_2 production in mitochondria and cytoplasm, respectively. Both probes were loaded at 5 μM for 30 min at 37 °C in Krebs ringer buffer (KRH: Hepes 25 mM at pH 7.4, NaCl 124 mM, KCl 5 mM, $MgSO_4$ 1.25 mM, CaCl2 1.25 mM, KH_2PO_4 1.25 mM, glucose 8 mM). Images were acquired at different points after toxin exposure with a DMI6000 inverted epifluorescence microscope (Leica) equipped with a 63× HCX PL APO oil immersion objective NA 1.4. Filter cubes (Chroma Technology) have an excitation range of 470/40 nm, a dichroic mirror 495LPXR, and an emission of 525/50 nm. Images were acquired with an Orca-Flash4 digital camera (Hamamatsu). Illumination was kept at a minimum to avoid ROS generation because of phototoxicity. To detect neuronal bulges, we took advantage of differential interference contrast microscopy. Fluorescence intensity quantification was carried out with ImageJ, and the statistical analysis with Prism (GraphPad).

Cell Treatments. CGNs (6 d in culture) plated onto 35-mm dishes (1.2 million cells per well) were exposed for 50–60 min to SPANs (6 nM) or to α-Ltx (0.1 nM) at 37 °C. In some experiments, neurons were preincubated for 30 min with cyclosporin A 5 μM before toxin addition. Supernatants or cell lysates were collected and then processed for real-time quantitative PCR (qPCR) or Western blot.

Primary SCs were exposed to different mitochondrial alarmins [H_2O_2 10–100 μM, Cyt c (R&D) 1 μg/mL, mtDNA 10 μg/mL] or to the toxins for different times and lysed in Lysis Buffer [Hepes 10 mM, NaCl 150 mM, SDS 1%, EDTA 4 mM, protease inhibitors mixture (Roche), and phosphatase inhibitor mixture].

Cocultures were treated with the toxins and then lysed after different points; in a set of experiments, 1,000 U per well catalase was added 5 min before intoxication and kept throughout the experiment; in another set, cocultures were incubated with the MEK1 inhibitor PD98059 (Cell Signaling; 80 μM) 1 h before toxins addition. Samples were then probed for p-ERK.

Immunofluorescence. After treatments, isolated SCs or cocultures were fixed for 15 min in 4% (wt/vol) paraformaldehyde (PFA) in PBS, quenched (0.38% glycine, 0.24% NH_4Cl in PBS), and permeabilized with 0.3% Triton X-100 in PBS for 5 min at room temperature (RT). After saturation with 3% (vol/vol) goat serum in PBS for 1 h, samples were incubated with primary antibodies [anti-Phospho-p44/42 MAPK (Cell Signaling), 1:1,000; anti- anti-NF200 (Sigma), 1:200; anti-S100 (Sigma), 1:1,000] diluted in 3% (vol/vol) goat serum in PBS overnight at 4 °C, washed, and then incubated with the correspondent secondary antibodies (Alexa-conjugated, 1:200; Life Technologies) for 1 h at RT. Coverslips were mounted in Mowiol and examined by confocal (Leica SP5) or epifluorescence (Leica CTR6000) microscopy.

In a set of experiments, CGNs were exposed to α-Ltx (0.1 nM, 50 min) or PMA (phorbol 12-myristate 13-acetate, 1 μg/mL, 20 min) and processed for immunofluorescence as described earlier. p47phox was detected by a monoclonal antibody (Santa Cruz; 1:200).

NMJ Immunohistochemistry. α-Ltx (5 μg/kg) or β-Btx (10 μg/kg) were diluted in 25 μL physiological saline (0.9% wt/vol NaCl in distilled water) and injected s.c. in proximity of the LAL muscle of anesthetized transgenic C57BL/6 male mice (expressing a cytosolic GFP under the *plp* promoter) (46, 47) of around 20–25 g. Control animals were injected with saline. LAL muscles were dissected at different points after injections and fixed in 4% (wt/vol) PFA in PBS for 30 min at RT. Samples were quenched, permeabilized, and saturated for 2 h in 15% (vol/vol) goat serum, 2% (wt/vol) BSA, 0.25% gelatin, 0.20% glycine, and 0.5% Triton X-100 in PBS. Incubation with the following primary antibodies was carried out for at least 48 h in blocking solution: anti-neurofilaments (mouse monoclonal, anti-NF200, 1:200; Sigma), anti-SNAP-25 (SMI81 mouse monoclonal, 1:200; Covance), and anti-CD68 (mouse monoclonal, 1:200; Santa Cruz). Muscles were then washed and incubated with secondary antibodies (Alexa-conjugated, 1:200 in PBS; Life Technologies). Nuclei were stained with Hoechst. For p-ERK detection incubation with the

primary antibody (anti-Phospho-p44/42 MAPK, 1:1,000; Cell Signaling) was carried out for 72 h and the tyramide signal amplification kit (Perkin-Elmer) was used (45).

To stain acidic compartments, LAL muscles collected after 4 h of intoxication were loaded ex vivo with LysoTracker Red DND-99 (1:5,000; Life Technologies) for 2–3 min (68) while being continuously perfused with oxygenated Neurobasal A medium (Life Technologies). Samples were then fixed and processed for indirect immunohistochemistry, as described earlier. Images were collected with a Leica SP5 confocal microscope equipped with a 63× HCX PL APO NA 1.4. Laser excitation line, power intensity, and emission range were chosen according to each fluorophore in different samples to minimize bleed-through.

Electrophysiological Recordings. Electrophysiological recordings were performed in oxygenated Krebs-Ringer solution on sham or α-Ltx-injected soleus muscles (α-Ltx 5 μg/kg, with or without 750 U catalase), using intracellular glass microelectrodes (WPI) filled with one part 3 M KCl and two parts 3 M CH_3COOK. In another set of experiments, muscles were locally injected with PD98059 (50 μg in DMSO) 1 h before α-Ltx injection.

Evoked neurotransmitter release was recorded in current-clamp mode, and resting membrane potential was adjusted with current injection to −70 mV. EJPs were elicited by supramaximal nerve stimulation at 0.5 Hz, using a suction microelectrode connected to a S88 stimulator (Grass). To prevent muscle contraction after dissection, samples were incubated for 10 min with 1 μM μ-Conotoxin GIIIB (Alomone).

Signals were amplified with intracellular bridge mode amplifier (BA-01X, NPI), sampled using a digital interface (NI PCI-6221, National Instruments) and recorded by means of electrophysiological software (WinEDR; Strathclyde University). EJPs measurements were carried out with Clampfit software (Molecular Devices).

Statistical Analysis. The sample size (N) of each experimental group is described in each corresponding figure legend, and at least three biological replicates were performed. Prism (GraphPad Software) was used for all statistical analyses. Quantitative data displayed as histograms are expressed as means ± SEM (represented as error bars). Results from each group were averaged and used to calculate descriptive statistics. Significance was calculated by Student's *t* test (unpaired, two-side). *P* values less than 0.05 were considered significant.

ACKNOWLEDGMENTS. We gratefully thank Dr. W. B. Macklin and Dr. T. Misgeld for providing the C57BL/6 transgenic mice strain and Dr. P. Caccin for the kind help with EM experiments. This work was supported by the Cariparo Foundation and the Provincia autonoma di Trento, Bando Grandi Progetti 2012 (to C.M.). M.R. is the recipient of Young Investigators Grant GR-2010-2320779 from the Italian Ministry of Health. C.J.C. is an Investigator with the Howard Hughes Medical Institute, and his contributions are supported by NIH Grant GM79465.

1. Pearn JH (1971) Survival after snake-bite with prolonged neurotoxic envenomation. *Med J Aust* 2(5):259–261.
2. Connolly S, et al. (1995) Neuromuscular effects of Papuan Taipan snake venom. *Ann Neurol* 38(6):916–920.
3. Kularatne SA, Senanayake N (2014) Venomous snake bites, scorpions, and spiders. *Handb Clin Neurol* 120:987–1001.
4. Duchen LW, Gomez S, Queiroz LS (1981) The neuromuscular junction of the mouse after black widow spider venom. *J Physiol* 316:279–291.
5. Dixon RW, Harris JB (1999) Nerve terminal damage by beta-bungarotoxin: Its clinical significance. *Am J Pathol* 154(2):447–455.
6. Chang CC, Chen TF, Lee CY (1973) Studies of the presynaptic effect of -bungarotoxin on neuromuscular transmission. *J Pharmacol Exp Ther* 184(2):339–345.
7. Rosenthal L, Zacchetti D, Madeddu L, Meldolesi J (1990) Mode of action of alpha-latrotoxin: Role of divalent cations in Ca2(+)-dependent and Ca2(+)-independent effects mediated by the toxin. *Mol Pharmacol* 38(6):917–923.
8. Hurlbut WP, Ceccarelli B (1979) Use of black widow spider venom to study the release of neurotransmitters. *Adv Cytopharmacol* 3:87–115.
9. Ceccarelli B, Hurlbut WP (1980) Vesicle hypothesis of the release of quanta of acetylcholine. *Physiol Rev* 60(2):396–441.
10. Südhof TC (2001) alpha-Latrotoxin and its receptors: Neurexins and CIRL/latrophilins. *Annu Rev Neurosci* 24:933–962.
11. Ushkaryov YA, Rohou A, Sugita S (2008) alpha-Latrotoxin and its receptors. *Handbook Exp Pharmacol* (184):171–206.
12. Rossetto O, Montecucco C (2008) Presynaptic neurotoxins with enzymatic activities. *Handbook Exp Pharmacol* (184):129–170.
13. Gutiérrez JM, Theakston RD, Warrell DA (2006) Confronting the neglected problem of snake bite envenoming: The need for a global partnership. *PLoS Med* 3(6):e150.
14. Pungercar J, Krizaj I (2007) Understanding the molecular mechanism underlying the presynaptic toxicity of secreted phospholipases A2. *Toxicon* 50(7):871–892.
15. Kasturiratne A, et al. (2008) The global burden of snakebite: A literature analysis and modelling based on regional estimates of envenoming and deaths. *PLoS Med* 5(11): e218.
16. Rigoni M, et al. (2005) Equivalent effects of snake PLA2 neurotoxins and lysophospholipid-fatty acid mixtures. *Science* 310(5754):1678–1680.
17. Paoli M, et al. (2009) Mass spectrometry analysis of the phospholipase A(2) activity of snake pre-synaptic neurotoxins in cultured neurons. *J Neurochem* 111(3):737–744.
18. Rigoni M, et al. (2007) Calcium influx and mitochondrial alterations at synapses exposed to snake neurotoxins or their phospholipid hydrolysis products. *J Biol Chem* 282(15):11238–11245.
19. Cull-Candy SG, Fohlman J, Gustavsson D, Lüllmann-Rauch R, Thesleff S (1976) The effects of taipoxin and notexin on the function and fine structure of the murine neuromuscular junction. *Neuroscience* 1(3):175–180.
20. Harris JB, Grubb BD, Maltin CA, Dixon R (2000) The neurotoxicity of the venom phospholipases A(2), notexin and taipoxin. *Exp Neurol* 161(2):517–526.
21. Tedesco E, et al. (2009) Calcium overload in nerve terminals of cultured neurons intoxicated by alpha-latrotoxin and snake PLA2 neurotoxins. *Toxicon* 54(2):138–144.
22. Duregotti E, Tedesco E, Montecucco C, Rigoni M (2013) Calpains participate in nerve terminal degeneration induced by spider and snake presynaptic neurotoxins. *Toxicon* 64:20–28.
23. Son YJ, Trachtenberg JT, Thompson WJ (1996) Schwann cells induce and guide sprouting and reinnervation of neuromuscular junctions. *Trends Neurosci* 19(7): 280–285.
24. Feng Z, Ko CP (2008) The role of glial cells in the formation and maintenance of the neuromuscular junction. *Ann N Y Acad Sci* 1132:19–28.
25. Krysko DV, et al. (2011) Emerging role of damage-associated molecular patterns derived from mitochondria in inflammation. *Trends Immunol* 32(4):157–164.
26. Zhang Q, et al. (2010) Circulating mitochondrial DAMPs cause inflammatory responses to injury. *Nature* 464(7285):104–107.
27. Zornetta I, et al. (2012) Envenomations by Bothrops and Crotalus snakes induce the release of mitochondrial alarmins. *PLoS Negl Trop Dis* 6(2):e1526.
28. Robitaille R (1998) Modulation of synaptic efficacy and synaptic depression by glial cells at the frog neuromuscular junction. *Neuron* 21(4):847–855.
29. Rochon D, Rousse I, Robitaille R (2001) Synapse-glia interactions at the mammalian neuromuscular junction. *J Neurosci* 21(11):3819–3829.
30. Auld DS, Robitaille R (2003) Perisynaptic Schwann cells at the neuromuscular junction: Nerve- and activity-dependent contributions to synaptic efficacy, plasticity, and reinnervation. *Neuroscientist* 9(2):144–157.
31. Todd KJ, Auld DS, Robitaille R (2007) Neurotrophins modulate neuron-glia interactions at a vertebrate synapse. *Eur J Neurosci* 25(5):1287–1296.
32. Todd KJ, Darabid H, Robitaille R (2010) Perisynaptic glia discriminate patterns of motor nerve activity and influence plasticity at the neuromuscular junction. *J Neurosci* 30(35):11870–11882.
33. Griffin JW, Thompson WJ (2008) Biology and pathology of nonmyelinating Schwann cells. *Glia* 56(14):1518–1531.
34. Son YJ, Thompson WJ (1995) Schwann cell processes guide regeneration of peripheral axons. *Neuron* 14(1):125–132.
35. Son YJ, Thompson WJ (1995) Nerve sprouting in muscle is induced and guided by processes extended by Schwann cells. *Neuron* 14(1):133–141.
36. Paulsen CE, Carroll KS (2010) Orchestrating redox signaling networks through regulatory cysteine switches. *ACS Chem Biol* 5(1):47–62.
37. Dickinson BC, Chang CJ (2011) Chemistry and biology of reactive oxygen species in signaling or stress responses. *Nat Chem Biol* 7(8):504–511.
38. Murphy MP, et al. (2011) Unraveling the biological roles of reactive oxygen species. *Cell Metab* 13(4):361–366.
39. Dickinson BC, Chang CJ (2008) A targetable fluorescent probe for imaging hydrogen peroxide in the mitochondria of living cells. *J Am Chem Soc* 130(30):9638–9639.
40. Dickinson BC, Peltier J, Stone D, Schaffer DV, Chang CJ (2011) Nox2 redox signaling maintains essential cell populations in the brain. *Nat Chem Biol* 7(2):106–112.
41. Rigoni M, et al. (2004) Snake presynaptic neurotoxins with phospholipase A2 activity induce punctate swellings of neurites and exocytosis of synaptic vesicles. *J Cell Sci* 117(Pt 16):3561–3570.
42. Gough DR, Cotter TG (2011) Hydrogen peroxide: A Jekyll and Hyde signalling molecule. *Cell Death Dis* 2:e213.
43. Kemmerling U, et al. (2007) Calcium release by ryanodine receptors mediates hydrogen peroxide-induced activation of ERK and CREB phosphorylation in N2a cells and hippocampal neurons. *Cell Calcium* 41(5):491–502.
44. Harrisingh MC, et al. (2004) The Ras/Raf/ERK signalling pathway drives Schwann cell dedifferentiation. *EMBO J* 23(15):3061–3071.
45. Napoli I, et al. (2012) A central role for the ERK-signaling pathway in controlling Schwann cell plasticity and peripheral nerve regeneration in vivo. *Neuron* 73(4): 729–742.
46. Mallon BS, Shick HE, Kidd GJ, Macklin WB (2002) Proteolipid promoter activity distinguishes two populations of NG2-positive cells throughout neonatal cortical development. *J Neurosci* 22(3):876–885.
47. Brill MS, Lichtman JW, Thompson W, Zuo Y, Misgeld T (2011) Spatial constraints dictate glial territories at murine neuromuscular junctions. *J Cell Biol* 195(2):293–305.
48. Angaut-Petit D, Molgo J, Connold AL, Faille L (1987) The levator auris longus muscle of the mouse: A convenient preparation for studies of short- and long-term presynaptic effects of drugs or toxins. *Neurosci Lett* 82(1):83–88.
49. Miller EW, Dickinson BC, Chang CJ (2010) Aquaporin-3 mediates hydrogen peroxide uptake to regulate downstream intracellular signaling. *Proc Natl Acad Sci USA* 107(36):15681–15686.

50. Rasola A, Sciacovelli M, Pantic B, Bernardi P (2010) Signal transduction to the permeability transition pore. *FEBS Lett* 584(10):1989–1996.
51. Rigoni M, et al. (2008) Snake phospholipase A2 neurotoxins enter neurons, bind specifically to mitochondria, and open their transition pores. *J Biol Chem* 283(49): 34013–34020.
52. Klyubin IV, Kirpichnikova KM, Gamaley IA (1996) Hydrogen peroxide-induced chemotaxis of mouse peritoneal neutrophils. *Eur J Cell Biol* 70(4):347–351.
53. Niethammer P, Grabher C, Look AT, Mitchison TJ (2009) A tissue-scale gradient of hydrogen peroxide mediates rapid wound detection in zebrafish. *Nature* 459(7249): 996–999.
54. Li L, Yan B, Shi YQ, Zhang WQ, Wen ZL (2012) Live imaging reveals differing roles of macrophages and neutrophils during zebrafish tail fin regeneration. *J Biol Chem* 287(30):25353–25360.
55. Conforti L, Gilley J, Coleman MP (2014) Wallerian degeneration: An emerging axon death pathway linking injury and disease. *Nat Rev Neurosci* 15(6):394–409.
56. Arthur-Farraj PJ, et al. (2012) c-Jun reprograms Schwann cells of injured nerves to generate a repair cell essential for regeneration. *Neuron* 75(4):633–647.
57. Lambert AJ, Brand MD (2009) Reactive oxygen species production by mitochondria. *Methods Mol Biol* 554:165–181.
58. Holmström KM, Finkel T (2014) Cellular mechanisms and physiological consequences of redox-dependent signalling. *Nat Rev Mol Cell Biol* 15(6):411–421.
59. Love NR, et al. (2013) Amputation-induced reactive oxygen species are required for successful *Xenopus* tadpole tail regeneration. *Nat Cell Biol* 15(2):222–228.
60. Tofaris GK, Patterson PH, Jessen KR, Mirsky R (2002) Denervated Schwann cells attract macrophages by secretion of leukemia inhibitory factor (LIF) and monocyte chemoattractant protein-1 in a process regulated by interleukin-6 and LIF. *J Neurosci* 22(15): 6696–6703.
61. Martini R, Fischer S, López-Vales R, David S (2008) Interactions between Schwann cells and macrophages in injury and inherited demyelinating disease. *Glia* 56(14): 1566–1577.
62. Court FA, Coleman MP (2012) Mitochondria as a central sensor for axonal degenerative stimuli. *Trends Neurosci* 35(6):364–372.
63. Patrushev M, et al. (2004) Mitochondrial permeability transition triggers the release of mtDNA fragments. *Cell Mol Life Sci* 61(24):3100–3103.
64. Frühbeis C, Fröhlich D, Krämer-Albers EM (2012) Emerging roles of exosomes in neuron-glia communication. *Front Physiol* 3:119.
65. Halstead SK, et al. (2005) Anti-disialosyl antibodies mediate selective neuronal or Schwann cell injury at mouse neuromuscular junctions. *Glia* 52(3):177–189.
66. Vinsant S, et al. (2013) Characterization of early pathogenesis in the SOD1(G93A) mouse model of ALS: Part II, results and discussion. *Brain Behav* 3(4):431–457.
67. Plomp JJ, Willison HJ (2009) Pathophysiological actions of neuropathy-related anti-ganglioside antibodies at the neuromuscular junction. *J Physiol* 587(Pt 16): 3979–3999.
68. Song JW, et al. (2008) Lysosomal activity associated with developmental axon pruning. *J Neurosci* 28(36):8993–9001.